Available online at www.sciencedirect.com
ScienceDirect
Journal of Molecular Catalysis A: Chemical 265 (2007) 32–41
JOURNAL OF MOLECULAR CATALYSIS A: CHEMICAL
www.elsevier.com/locate/molcata

Atoms in molecules theory for exploring the nature of the MoS_2 catalyst edges sites

Yosslen Aray *, Jesus Rodríguez

Centro de Quimica, IVIC, Apartado 21827, Caracas 1020A, Venezuela

Received 12 July 2006; received in revised form 8 September 2006; accepted 14 September 2006
Available online 23 September 2006

Abstract

The nature of the MoS_2 catalyst edge was studied using the atoms in molecules theory. The network of bond paths describing the atomic connectivity has shown that the exposed graph of this edge results from the packing of polyhedra, with six vertexes and four faces, located at the Mo edges and polyhedra, with five vertexes and three faces, located at both sides of the S edge. The former polyhedra are bonded by a much bigger electron density suggesting a relationship between this fact and the smaller necessary energy to create a sulfur vacancy on the S edges than the Mo edges. Additionally, we have found that potential active sites on the catalyst surface can be localized visualizing the outermost interatomic surfaces.

Keywords: Molybdenum sulfide catalyst; Atoms in molecules theory; Density functional theory

1. Introduction

Transition metal sulfides (TMS) belong to a very important class of catalysts characterized by being stable under hard conditions in hydrodesulfurization (HDS), hydrodenitrogenation (HDN) and hydrogenation reactions [1–3]. In these processes, the surfaces of the sulfides are reduced by sulfur elimination using large excess of hydrogen at temperatures ranging from 573 to 673 K creating coordinatively unsaturated sites (CUS) or vacancies around the metals. CUS behave as an electron-withdrawing site whose properties may be regarded as a Lewis acid type center interacting with electrodonating organic substrates [4–6]. The nature of these sites is suggested to be intimately related to the metal sulfur bond strength [2,4,5,7,8]. Basic studies support the view that differences in catalytic activities, are related to variations in the concentration of CUS (the Lewis acid sites), which in turn depend on the metal-sulfur bond strength [9–19]. Based on ab initio calculations [2,7], a bond energy model (BEM), which describes the variation in the metal-sulfur bond energies for all the transition metal sulfides was developed. It was found that the trends in the calculated bond energies follow closely the trend in the HDS activities. Studies using X-ray absorption fine structure (EXAFS) have established that the active Mo atom is present as small MoS_2-like nanostructures [20,21]. Adsorption and activity experiments [22,23] have revealed that the active sites reside at the edges of the MoS_2 structures and a recently high-resolution scanning tunneling microscopy (STM) and density-functional theory (DFT) studies [24] have shown that the MoS_2 nanoclusters adopt a hexagonal shape exposing two different types of edges, Mo edges covered with S monomers and fully sulfur-saturated S edges.

The "atoms in molecules theory" (AIM) of Bader et al. is very useful to obtain the chemical information from the charge density [25–34]. AIM is a firm, rigorous and quantum mechanically well-defined theory based on observables such as the electron density or energy density fields. Most modern theories of bonding are based, in one way or another, on the partition of charge (or electronic density) among the different nuclear centers under study, usually by means of Mulliken—i.e., projected density of states in solid-analysis. In this way, an important amount of the interpretative models of chemical behavior are based on concepts that are known to be very badly defined, and to give answers extremely dependent on a whole hierarchy of approximations [32]. AIM provides a quantitative link between the total electron density (regardless of how it was generated: calculated or experimental) and the all important physical properties of a

* Corresponding author. Tel.: +58 212 5041356; fax: +58 212 5041350.
E-mail address: yaray@ivic.ve (Y. Aray).

1381-1169/$ – see front matter © 2006 Elsevier B.V. All rights reserved.
doi:10.1016/j.molcata.2006.09.034

molecule, bypasses the wave function in the analysis. AIM is a orbital concept free methodology. In particular, it provides a rigorous definition of chemical bonds and geometrical structure for all types of molecules and solids and has proven useful in the analysis of physical properties of insulators, pure metals and alloys [4–8]. High-quality experimental densities of minerals [35–39], covalent [40], metallic [41], and molecular crystals [42–45] have been analyzed in terms of AIM concepts. Theoretical calculations on simple metals [31,46–48], alloys and intermetallic phases [49–53], molecular [48,54–56], covalent and ionic crystals have also been reported [32,39,40,48,57,58]. AIM also provides a rigorous topological and quantum mechanical definition of atoms that have been identified with the atom of chemistry. These atoms have shown to recover the essential notions associated with the atomic concept: (i) the atomic properties are characteristic and additive to yield the corresponding values for the total system; (ii) they are as transferable from one system to another as are the forms of the atoms in real space; that is, as transferable as are the atomic charge distribution. In particular, atomic and group properties predicted in this manner have been shown to recover the experimentally determined contributions to the volume, energy, polarizability, and magnetic susceptibility [25]. This theory makes use of the total electron density, $\rho(\mathbf{r})$, of a molecule or solid to determine its topology [26,33], which is characterized by its critical points (CPs): maxima, minima and saddles points. In general, $\rho(\mathbf{r})$ exhibits local maxima only at the nuclear positions and a saddle point called a bond critical point between each pair of bonded nuclei. The connection between the topology of the electron density and the chemical and structural stability of isolated molecules and crystals has been well established [26,32,33]. Specially, it has been observed that the strength of the bonding between a given pair of atoms in a molecule correlates with the values of the electron density at the bond critical point, ρ_b [26]. A simple relationship between the binding energy and ρ_b in periodic solids has also been reported [19,28,31,59]. In order to continue improving the understanding of HDS catalysts, in the present paper we have explored the nature of the structure of the MoS_2 edge using the AIM theory, its relationship to the creation energy and position of CUS on the catalyst.

2. The AIM theory

The topological properties of a crystal charge distribution are summarized by its critical points (CP) [25,34]. These are points where the gradient vector field, $\nabla\rho(\mathbf{r})$ vanishes, and they are classified by the $\rho(\mathbf{r})$ curvatures or three eigenvalues λ_i ($i = 1, 2$, and 3) of the Hessian matrix ($H_{ij} = \partial^2\rho(\mathbf{r})/\partial x_i \partial x_j$). They are labeled by their rank (number of nonzero eigenvalues) and signatures (excess number of positive over negative eigenvalues) and correspond to maxima (3, −3), minima (3, +3), and saddle points (3, +1) and (3, −1). Every CP has a characteristic pattern of trajectories or gradient paths of $\rho(\mathbf{r})$. The trajectories originate and end at critical points. Only the (3, −3) points are three-dimensional trajectory attractors: trajectories only terminate at this CP. The (3, −3) points occur generally at the nuclear positions so that each nucleus is a three-dimensional point attractor in the vector field $\nabla\rho(\mathbf{r})$. The region traversed by the gradient paths, which terminate at a given attractor defines the basin of the attractor. A (3, −1) CP, the bond critical point (b), is found between every pair of neighboring nuclei. It represents both local maxima in two directions and a local minimum in the third direction. The gradient paths associated with the negative eigenvalues at the (3, −1) point terminate at this CP and define the interatomic surfaces, IAS, that partition the crystal into unique fragments (the atomic basins). In general, the boundary of an atom in a crystal consists of the union of its interatomic surfaces. The unique pair of trajectories associated with the positive eigenvalue of the (3, −1) CP originates at this point and terminate at the neighboring attractors. These two unique gradient paths define a line (the bond path) linking the nuclei (n), along which the charge density is a maximum with respect to any neighboring line. The network of bond paths defines a graph, namely the crystal graph, which describes the atomic connectivity and structure within a crystal cell. The other CPs occur as a consequence of the geometrical arrangements of bond paths and they define the remaining elements of crystal structure, namely rings and cages. If the bond paths are linked to form a ring of bonded atoms then a (3, +1) CP is found in the interior of the ring. The eigenvectors associated with the two positive eigenvalues of the (3, +1), a ring (r) CP, generate an infinite set of gradient paths which originate at the CP and define a surface, called the ring surface. All of these trajectories terminate at the ring nuclei or at the bond CPs whose bond paths form the perimeter of the ring. The single negative eigenvector of the ring CP generates a pair of gradient paths, which terminate at the CP and define a unique axis perpendicular to the ring surface at the critical point. The (3, +3) or cage (c) CPs are located inside a cage nuclear arrangement. The charge density is a local minimum at a cage CP and in crystals it is the main source of trajectories of $\nabla\rho(\mathbf{r})$: trajectories only originate at such CPs and terminate at nuclei, bond or ring CPs. The type and numbers of CPs for an extended system [28,33] satisfy the Morse invariant relationships:

$$n - b + r - c = 0 \tag{1}$$

3. Computational methodology

$\rho(\mathbf{r})$ was calculated by means of the Dmol^3 [60,61] program using the Kohn–Sham Hamiltonian with the gradient-corrected Perdew–Becke–Ernzerhof (PBE) exchange-correlation functional [62]. Dmol^3 calculates variational self-consistent solutions to the DFT equations, expressed in an accurate numerical atomic orbital basis. The solutions to these equations provide the molecular electron densities, which can be used to evaluate the total electrostatic potential of the system. The numerical double-zeta plus polarization basis set DNP [60,61] was used in all calculations. DMol^3 uses DFT to obtain high accuracy while keeping the computational cost fairly low for an ab initio method. Six special $\boldsymbol{k}$ points generated using a [4 3 1] mesh along the three cell axes and the Monkhorst–Pack scheme [60,61] were used to integrate the wavefunction in the reciprocal space. The topology of $\rho(\mathbf{r})$ was determined using a reported implementation [63] of the Newton–Raphson and fifth-order

Cash–Karp Runge–Kutta methods in a $\rho(\mathbf{r})$ three-dimensional grid.

4. Catalyst models

MoS_2 bulk is a layered type crystal whose lattice is described by the hexagonal space group $P63/mmc$ with $a = b = 3.160$ Å and $c = 12.294$ Å [64]. Its crystal structure belongs to a family of polytypic structures with close-packed triangular double layers of S with Mo atoms arranged in the trigonal-prismatic holes of the S double layers. Mo atoms occupy [65] the 2*c* Wyckof positions with coordinates (1/3, 2/3, 1/4) and the S atoms the position 4f with coordinates (2/3, 1/3, 0.371). Each Mo atom is bonded to six S atoms in a trigonal-prismatic arrangement. The closest S–S distances are across the double layer and within the close-packed layers; the interlayer S–S distances are considerably larger and of van der Waals type. The morphology of the catalysts [4] can be depicted as small MoS_2 particles (crystallites) dispersed at the surface of the support (usually gamma-alumina). These particles have an average size of about 600 ± 200 Å^2 and its reactivity depends on preferential exposed faces or planes. Cleveage of the bulk structure parallel to (0 1 0) plane produces the well known edge surface exposing coordinatively unsaturated molybdenum or sulfur atoms. Each of the exposed Mo atoms is coordinated to four sulfur atoms, while each of the terminal sulfur atoms is coordinated to two Mo atoms. Several studies have shown that the bare Mo edge terminating in a row of undercoordinated Mo atoms is very unfavorable and thus such edges will have a high affinity toward S adsorption. The real morphology of the MoS_2 catalyst active sites has been deduced from experimental and theoretical studies. STM allows direct imaging of catalytically relevant surface structure on the atomic scale. By studying [24] a realistic HDS model system consisting of a few-nanometer-wide gold-supported MoS_2 particles it was shown that morphology of the nanoparticles is sensitive to sulfiding and reaction conditions; this means, triangles under heavy sulfiding conditions or truncated hexagons under more sulfo-reductive conditions resembling HDS conditions. These hexagonal clusters expose the basal plane and two different types of edges: Mo edges covered with S monomers and fully saturated S edges [24]. Different models have been used to study the edge structure of MoS_2 catalysts using DFT methods: cluster models including a finite number of atoms [24,66], a single S–Mo–S periodic slab [67,68] and a larger slab model containing two S–Mo–S sheets exposing Mo- and S-edges alternatively [24,29,69–73]. From these studies a clear picture of the MoS_2 edge structures has emerged: the most external Mo atoms of the Mo edge contain 50% sulfur coverage with each sulfur atom bridged to two neighboring molybdenum atoms. A significant reconstruction of the Mo edge takes place: the bridged S atoms are to be shifted

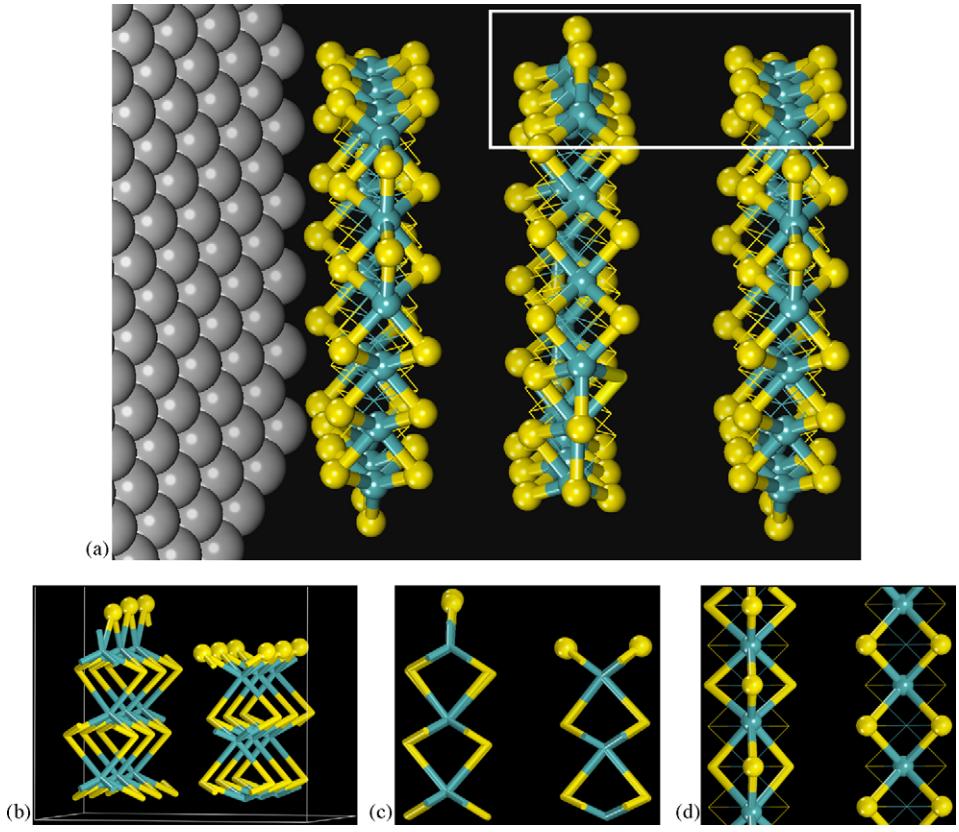

Fig. 1. (a) Balls and cylinders model showing a side view of a hypothetical MoS_2 nanoparticle that simulates the particles of Ref. [4]. Blue and yellow spheres denote the Mo and S atoms on the edges, respectively. A white rectangle highlights the structure of the site that interacts with the incoming molecules. (b) Side-view. (c) At the *YZ* plane. (d) Top-view (*XZ* plane) of the MoS_2 edges unit cell. Blue and yellow cylinders denote the Mo and S atoms, respectively. The S edges are on the right of each unit cell and expose six S atoms by cell. (For interpretation of the references to colour in this figure legend, the reader is referred to the web version of the article.)

by half a lattice constant relative to the bulk S lattice, and they move down to a bridging position in-plane with the Mo lattice. The S edges remain fully sulfided and a maximum Mo coordination to six sulfur atoms is achieved in one configuration where the edge is terminated by a row of sulfur atoms positioned in a bridge position close to those expected from bulk-terminated MoS_2. Both edge geometries lead to a coordination number of six for the outermost molybdenum atoms and two for the corresponding sulfur atoms. High-resolution electron microscopy studies of silica-supported Mo based catalysts have shown that the morphology of the catalyst can be depicted as small particles dispersed on the surface of the support with an average size of 29 Å (mean diameter) and three slabs in width [4]. Fig. 1a shows a model of such particle and the structure of the particle edge is highlighted by means of a white square.

In the present paper, we will study the larger periodic slab model (Fig. 1b–d) that exposes alternating layers of Mo and S edges denoting nanoparticles several layers wide. The super cell (9.480 Å × 12.294 Å × 36.000 Å) of this surface exhibits three and six bridged S atoms above the Mo and S edges, respectively. It consists of two S–Mo–S sandwiches stacked in the Z direction: each slab contains three layers of Mo atoms in the Y direction and three in the X direction initially having the same structure of the surface built directly from the bulk. This unit is periodically repeated in the X and Z directions. Vacuum layers thicker than 15 Å were used to ensure that there were no interactions between adjacent slabs. The geometry of this model was optimized using algorithms included in the Dmol^3 program [60,61]. The two upper rows were allowed to relax while the atoms of the lower ones were kept fixed at their optimized bulk positions to simulate bulk constrains.

5. Results

The $\rho(\mathbf{r})$ topology for the MoS_2 edge model (Fig. 2) has shown the presence of almost the same type of CPs [63] as that of the bulk case: Mo–S (gray spheres) and S–S bond critical points (white cylinder), four-membered ring CPs, trigonal prism-like

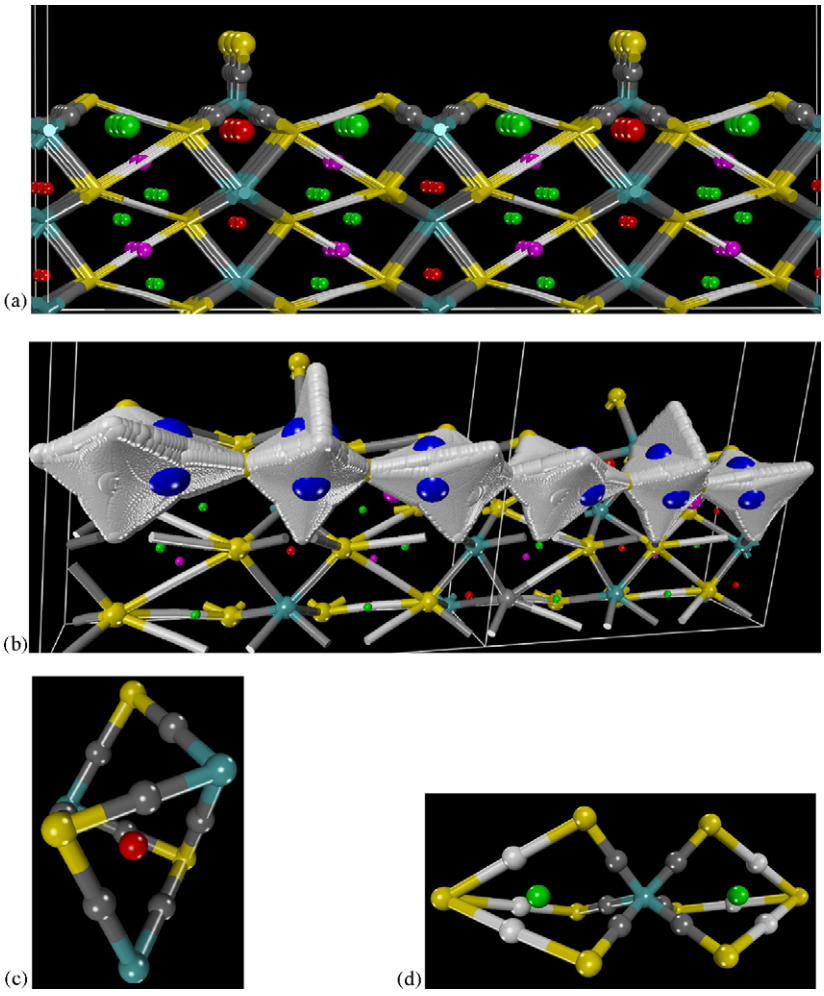

Fig. 2. (a) Side-view of a balls and cylinders model illustrating the $\rho(\mathbf{r})$ bond and cages critical points of the MoS_2 edge. Light blue and yellow balls denote the Mo and S atoms, respectively. Dark gray spheres (or cylinders) and white cylinders denote the Mo–S and S–S bond CPs, respectively. Red, green and pink spheres denote the cage CPs. Big spheres highlight the outermost CPs. (b) Side-view of the outermost polyhedra defined by ring surface (white surfaces) delineated by the gradient paths that originate at the ring CPs (dark blue spheres) and end at the nuclei. (c) {6, 8, 4} polyhedrum defined for the outermost S atoms on the metal edge. (d) Most external {5, 6, 3} polyhedra bonded to the exposed Mo atoms of the sulfur edge. (For interpretation of the references to colour in this figure legend, the reader is referred to the web version of the article.)

Table 1
Topological Properties (au) of $\rho(\mathbf{r})$ at the outermost Critical Points for MoS_2 edges

Edge	Critical point	λ_1	λ_2	λ_3	ρ_b
Sulfur	Mo–S *b*	−0.1011	−0.0943	0.3054	0.0916
Sulfur	Four-membered 2Mo–2S *r*	−0.0068	0.0216	0.0496	0.0323
Sulfur	Four-membered 1Mo–3S *r*	−0.0023	0.0072	0.0127	0.0061
Sulfur	Red *c* (Fig. 2)	0.0066	0.0122	0.0733	0.0311
Both	Green *c* (Fig. 2d)	0.0015	0.0051	0.0087	0.0054
Both	Pink *c*	0.0012	0.0026	0.0026	0.0029
Both	S–S *b*	−0.0047	−0.0043	0.0307	0.0087
Mo	Mo–S *b* new	−0.1010	−0.0962	0.3215	0.0926
Mo	Red *c* new (Fig. 2c)	0.0050	0.0117	0.0690	0.0297

b, *r*, and *c* denote bond, ring and cage critical points.

cage (small red spheres), distorted trigonal prism cage (green spheres) and 14-faced cages (pink spheres). A new kind of cage (big red spheres) capped by the outermost sulfur atoms on the metal edge (big yellow spheres) is the main difference with the bulk CPs. The S–S bond CPs are located just at the middle of each pair of neighbor MoS_2 sheets, in the interlayer region, bonding the neighbor layers. The entire set of critical points defines specific bonding polyhedra, the packing of which gives rise to the MoS_2 (0 1 0) surface structure. The topology of these polyhedra is determined only by the numbers of vertexes, edges and faces. Vertexes are the nuclei ($\nabla\rho(\mathbf{r})$ trajectories attractors), edges are the bond paths or attraction lines between nucleus and bond CPs, and each face is an attraction surface of the nucleus, i.e. a ring surface (Fig. 2b). As we can see, the nature of these polyhedra is determined by the $\nabla\rho(\mathbf{r})$ trajectories attractor character of the vertexes. A convenient notation for them [29] is {vertexes number, edge number, face number}. The outermost red cages describe {6, 8, 4} polyhedra (Fig. 2c). Thus, the network of bond paths describing the atomic connectivity shows that the crystal graph of the exposed structure for the MoS_2 surface results from

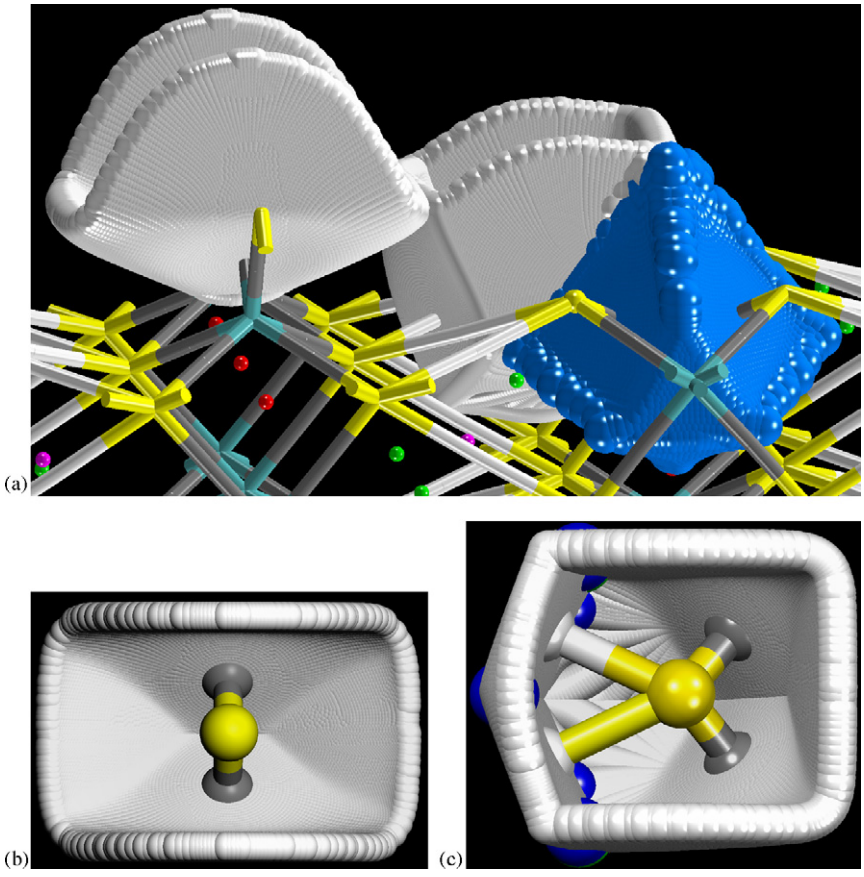

Fig. 3. (a) Atomic basins for the outermost Mo atom on the sulfur edge (blue polyhedron) and S atoms (white open structure) on the metal (left) and sulfur (right) edges. Note that these S atoms are open system and a practical definition is to cap them with an isosurface of $\rho(\mathbf{r})$. (b) Top-view of the IAS defining the basin of the outermost S atoms on the Mo edge. (c) Top-view of the corresponding basin of the outermost S atoms on the S edge. Pink, red and green spheres denote cage CPs while white, gray cylinders (or spheres) denote S–S and Mo–S bond CPs, respectively. Light blue and yellow cylinders denote Mo and sulfur atoms, respectively. (For interpretation of the references to colour in this figure legend, the reader is referred to the web version of the article.)

the packing of these {6, 8, 4} polyhedra and {5, 6, 3} polyhedra with a green cage just at the middle (Fig. 2d). Each {6, 8, 4} polyhedron is defined by eigth Mo–S bond paths with an average ρ_b value (Table 1) of 0.0926 au and contains a cage CP with a ρ_c value of 0.0297 au while the {5, 6, 3} polyhedra are defined by three Mo–S bond paths with an average ρ_b value of 0.0916 au and three S–S bond with ρ_b value of 0.0087 au and contain a cage with ρ_c value of 0.0054 au. Therefore, the former polyhedra whose nuclei are bonded by a much bigger electron density should be more stable than the {5, 6, 3} polyhedra.

An alternative way to study the crystal packing is given by the atomic basins, i.e., the volume spanned by the paths ending at a given nucleus. Basins are topologically equivalent to polyhedra, in the sense that they have faces, edges and vertexes, and they satisfy Euler's relationship (faces − edges + vertexes = 2) [32]. Unlike polyhedra, however, basins tend to have rather curved edges and faces. Vertexes are cage CPs or $\rho(\mathbf{r})$ minima, i.e., $\nabla\rho(\mathbf{r})$ trajectories source, edges are the attraction lines between cage and ring CPs and each faces is the attraction surface of a bond CP, i.e., the IAS. For this case, the nature of the packing units is determined by the $\nabla\rho(\mathbf{r})$ trajectories source character of the vertexes. A vision 3D of the IAS and the basin for the outermost Mo and S atoms are given in Fig. 3. The basin for the outermost Mo atoms is bordered by six Mo–S inter atomic surfaces. A set of seven cages (the paths that originate at the cages and terminate at the Mo nuclei outline its associated basin) defines these Mo atoms. In a similar way to the bulk case [63], the internal IAS are generated by the paths that originate at four cages while the outermost ones are defined by only two cages and by the paths coming from the infinite (the open space) and terminate at the bond CPs. The basin for the outermost S atoms on the Mo edge and on the sulfur edge is bordered by two and four Mo–S IAS, respectively. Fig. 4 shows a top view of several of those S basins. As we can see, the Mo atoms are totally covered by the sulfur atoms, which obstruct the access of incoming molecules like dibenzothiophene that contains the pollutant sulfur atoms. This result agrees with the known inactivity of this kind of sites like to the basal plane that only exposes sulfur atoms. Therefore, we have to create vacancies or CUS on this surface by a reduction process in order to generate available Lewis acidic sites. Usually [24c] H_2 reacts with surface sulfur atoms to create a vacancy and produce H_2S and therefore, the energy to create a sulfur vacancy can be calculated using the following equilibrium:

$$\text{surface} - \text{S} + \text{H}_2 \Leftrightarrow \text{surface} - \square + \text{H}_2\text{S}. \quad (2)$$

Thus, the creation energy, CE, of a sulfur vacancy is given by the expression:

$$\text{CE} = E(\text{surface} - \square) + E(\text{H}_2\text{S}) - E(\text{surface} - \text{S}) - E(\text{H}_2) \quad (3)$$

The energy of each sulfur removal has been reported and the stability of each surface has been deduced using a DFT methodology based in pseudo potentials and plane wave basis sets [24c,74]. Recently, the CE and the Lewis acidity strength of sulfur vacancies or coordinative unsaturated sites on the MoS_2 edges were studied using density functional theory for periodic systems and an electrostatic potential based methodology [75]. On the sulfur edge, the gradual removal of the six S atoms of the cell (Fig. 1b) was studied and for each case the geometrical optimization of the reported most stable configuration was carried out. For the Mo edge, the gradual removal of the three S atoms (Fig. 1b) ending with the full exposure of the underlying Mo atoms was also studied. The Lewis acidity strength of these sites

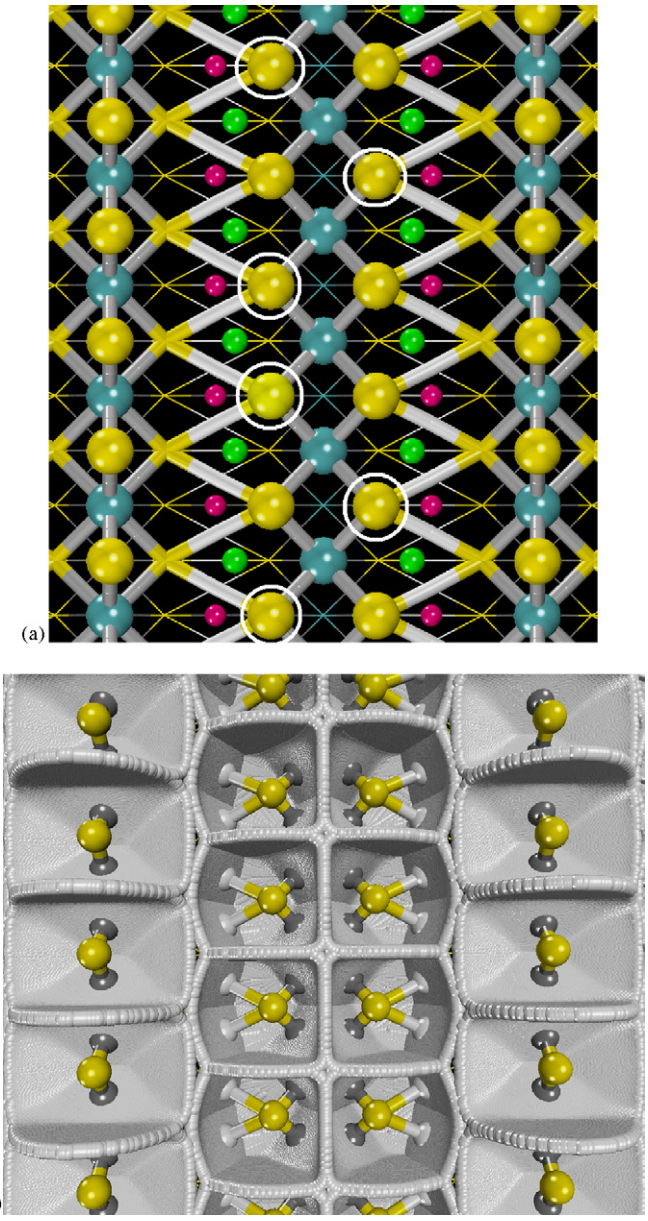

Fig. 4. (a) Top-view of the balls and cylinders model of Fig. 2 illustrating the $\rho(\mathbf{r})$ bond and cages critical points of the MoS_2 edge. Light blue and yellow spheres denote the outermost Mo and S atoms, respectively. Dark gray and white cylinders denote the Mo–S and S–S bond CPs, respectively. Green and pink spheres denote cage CPs. Big yellow spheres denote the outermost S atoms on the Mo edge. White circle highlight the S atoms that will be remove to create the active site. (b) Top-view of the MoS_2 edge surface periodic model showing the IAS definig the basins of the outermost S atoms. Note that the Mo atoms are totally encapsulated by the external S atoms. (For interpretation of the references to colour in this figure legend, the reader is referred to the web version of the article.)

can be particularly explored using the electrostatic potential, $V(\mathbf{r})$, which let us directly to determine where the electron-rich sites in a molecule or crystal are localized [76–80]. In that work, mapping the $V(\mathbf{r})$ values onto colors on the 0.002-electron/bohr^3 contour isosurface of the molecular electronic density $\rho(\mathbf{r})$, to identify the host sites in which nucleophiles (most negative zone) and electrophiles (most positive zone) should bind, was used to explore the Lewis acid sites on the MoS_2 edges. Additionally, to quantify the active sites susceptibility, the local minimum and maximum $V(\mathbf{r})$ values at the determined host zones were also determined. As a compromise of Lewis acidity strength and energetic, the site obtained by removing three S atoms from the cell, just on the S edge; with 50% of sulfur coverage was suggested to be the most hydrodesulfurization active site, AS. [75] Removal of just one S atom on the Mo edge costs 153.345 kJ/mol [75] while the creation of AS only needs 72.579 kJ/mol. This result confirm the previously suggested bigger stability of the {6, 8, 4} polyhedra on the Mo edges than the {5, 6, 3} polyhedra on the S edges. Removal of each S atom of the S edge destroys two {5, 6, 3} polyhedra; therefore, the destruction of six these last polyhedra to create AS costs half of the necessary energy to destroy just one {6, 8, 4} polyhedron to create a vacancy on the Mo edge.

The $\rho(\mathbf{r})$ topology for AS is shown in Fig. 5a. This site is obtained by removing three S atoms (highlighted by circles in Fig. 4a) from the cell, just on the S edge; the remaining three S atoms occupy again bridging positions between the Mo sites. However, in contrast to the Mo edge, the S atoms are tilted such as to conform as far as possible the bonding Mo–S network existing in the solid. The Mo–S distances at the S edge vary between 2.29 and 2.32 and are shorter than the Mo–S distances (2.40) of the surface without vacancies. The S atoms with the shortest Mo–S distances (two by cell) show only one S–S bond (Fig. 5a) completing tri-coordinated S atoms while the other S atom of the cell preserves the two S–S bonds located in the inter-edge space forming four-coordinated atoms. Holes (denoted as white rectangles in Fig. 5a) in the bond path network, between each pair of consecutive four-coordinative S atoms, can be observed.

The basins for the outermost S atoms of AS are shown in Fig. 5b. As we can see, compared to the surface without vacancies (Fig. 4b), the basins on the S edge have suffered a drastic change in their shape. These atoms spread to occupy the space liberated in the vacancies and adopt a triangular form like an arrow head. The base of each triangle is defined by the S–S IAS while the opposite angle (head point) penetrates inside the vacancy, occupying the space liberated by the removed S atoms, ending at the middle of the network bond path hole. The region around these head points (highlighted by rectangles in Fig. 5b) should be the sites with smaller sulfur electronic density on the surface allowing the access to the Mo atoms (the Lewis acid sites). This fact can be easily checked by means of the electrostatic potential. This parameter let us directly to visualize the stronger Lewis acid sites (most positive zone) on a surface mapping the $V(\mathbf{r})$ values onto colors on the 0.002 electron/bohr^3 isosurface of $\rho(\mathbf{r})$. Fig. 6 shows the superposition of this color map on the exposed S atom basins of the MoS_2 edges model. Starting from the most negative $V(\mathbf{r})$ values (see caption of

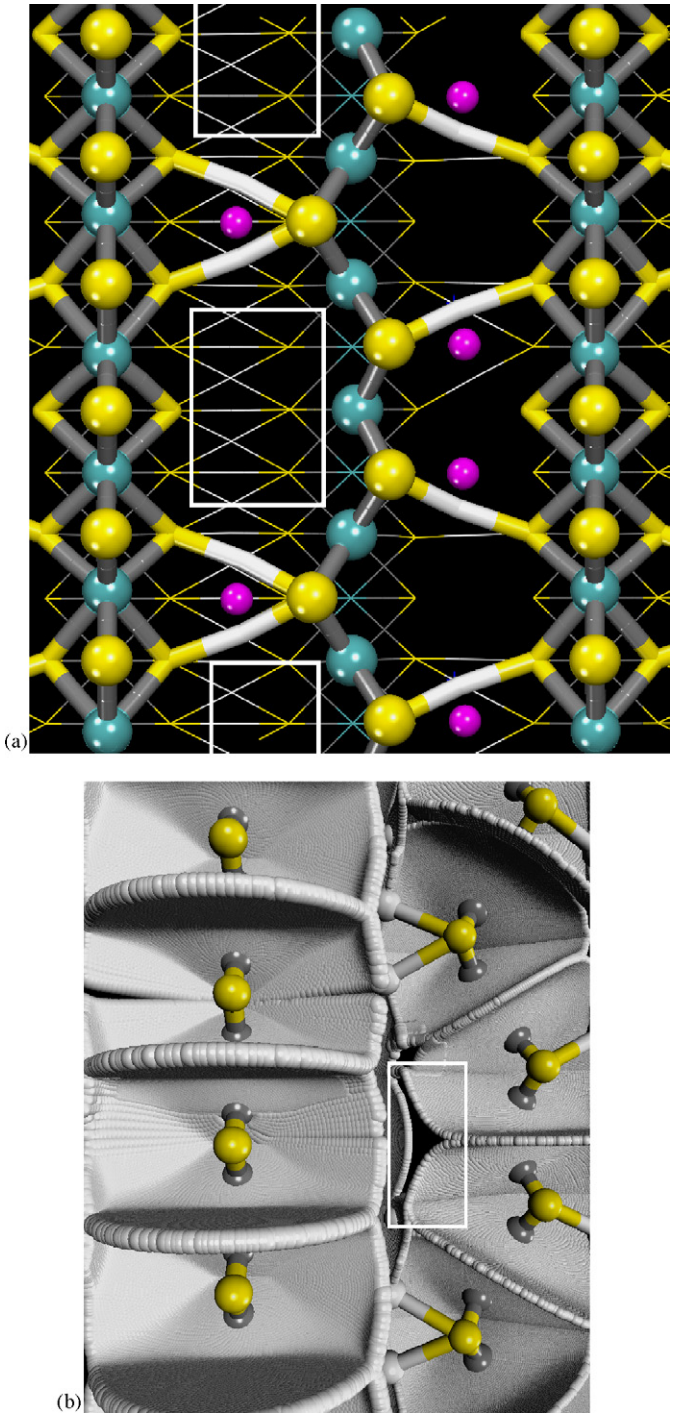

Fig. 5. (a) Top-view of a balls and cylinders model illustrating the bond and cages $\rho(\mathbf{r})$ critical points of the active site. Light blue and yellow spheres denote the outermost Mo and S atoms, respectively. Dark gray and white cylinders denote the Mo–S and S–S bond CPs, respectively. Pink spheres denote cage CPs. Note that holes (highlight by white rectangles) in the bond path network have appeared. (b) Top-view of active site showing the IAS defining the exposed basin of the outermost S atoms. Holes in the interatomic surfaces (highlight by white rectangles) suggest the site where the Mo atoms are most accessible to the incoming molecules. (For interpretation of the references to colour in this figure legend, the reader is referred to the web version of the article.)

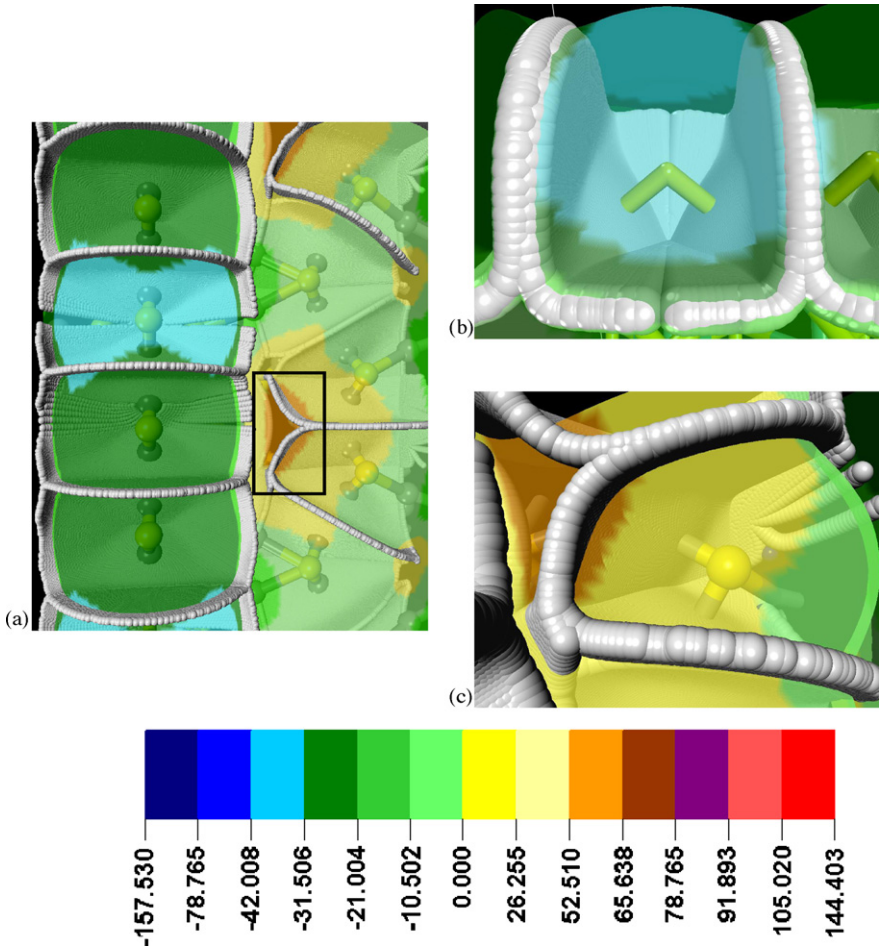

Fig. 6. (a) Top view of the 0.002 au contour of $\rho(\mathbf{r})$ mapping the $V(\mathbf{r})$ field values onto colors and placed over the IAS definig the basin of the outermost sulfur toms. The color map tab at the bottom is, blue jay (−157.530 to −78.765 kJ/mol), blue heaven (−78.765 to −42.008 kJ/mol), light blue (−42.008 to −31.506 kJ/mol), dark green (−31.506 to −21.004 kJ/mol), green (−21.004 to −10.502 kJ/mol), light green (−10.502 to 0.000 kJ/mol), yellow (0.000 to 26.255 kJ/mol), yellow cream (26.255 to 52.510 kJ/mol), orange (52.510 to 65.638 kJ/mol), brown (65.638 to 78.765kJ/mol), purple (78.765 to 91.893 kJ/mol), light red (91.893 to 105.020 kJ/mol) and red (105.020 to 144.403 kJ/mol). A black square indicate the most positive zones on the $\rho(\mathbf{r})$ contour, respectively. (b) and (c) Side-view of the basin of the outermost sulfur atoms on the Mo edge and the S edge, respectively. The 0.002 au contour of $\rho(\mathbf{r})$ is used to define the border of these open atoms. $V(\mathbf{r})$ mapped on this border allows us to locate the stronger Lewis acid sites. (For interpretation of the references to colour in this figure legend, the reader is referred to the web version of the article.)

Fig. 6), three kinds of blue and three kinds of green denote the most negative ones while two kinds of yellows and one orange denote the positive $V(\mathbf{r})$ values. The orange region corresponds to the most positive site and as we can see in Fig. 6, it perfectly matches with the hole where two sulfur basin head point almost converge.

The effect on the stability of the MoS_2 edge surface of the reaction conditions such as temperature and partial pressure of H_2 and H_2S present in the surrounding atmosphere has been reported [72] using a combination of periodic DFT calculations and thermodynamic analysis. It was found that the sulfur coverage of both kinds of edges is strongly dependent on the H_2S/H_2 partial pressure ratio in the surrounding gas phase. For high pressure of H_2S the surface with six sulfur atoms at the S edge (Fig. 2) is the most stable surface. For high hydrogen pressure, that should correspond to the catalyst working conditions, AS should be the most stable surface. Kinetic modeling [73] of H_2S removal from the edge surfaces has shown that is possible to extract one S atom per Mo edge creating a very small number of vacancy/cell on this edge. However, a previous study [75] of the MoS_2 edge vacancies Lewis acidity strenght has shown that just one CUS on the Mo edge creates weak Lewis acid sites, even weaker than AS. In order to obtain very acid sites at least two and four S atoms have to be removed at the Mo and S edges, respectively, but to a cost of a huge creation energy. Therefore, the present results suggest the presence of available Lewis acidic sites on the MoS_2 catalyst such as AS at the catalytic reaction conditions. In agree with experimental results [4], these sites should be weak Lewis acid sites.

Exposed atoms, such as an atom in an isolated molecule, has considerable open parts that extend to infinity. These atoms are open or unbounded at the exterior of the surface and a practical definition [10] is to cap the atom with an isosurface of the electron density with small $\rho(\mathbf{r})$ value representing the van der Waals envelope of the system. The 0.002 electron/bohr^3 contour of $\rho(\mathbf{r})$ shown in Fig. 6 just defines the border of the outermost sulfur atoms of the (0 1 0) MoS_2 surface. Fig. 6b and c shows a side-view of the atomic shape of these sulfur atoms. It is worthwhile

to note that the stronger Lewis acid sites are located between the sulfur atoms just at the bottom of the $\rho(\mathbf{r})$ 0.002 contour valley. This is the region where the Mo atoms are most accessible to the incoming molecules.

6. Concluding remarks

There is a deep relationship between the vacancy creation energy, i.e. the necessary energy to remove exposed sulfur atoms in the MoS_2 surface and the nature (number of bond paths and the $\rho(\mathbf{r})$ value at the bond and cage CPs) of the exposed polyhedra defining the surface graph. Additionally, the structure and shape of the basins of the exposed sulfur atoms allow us to visualize and locate the Lewis acid site on this surface.

Acknowledgement

This work was supported by the grant G-2000001512 from the CONICIT (Consejo Nacional de Investigaciones Científicas y tecnológicas) of Venezuela.

References

[1] O. Weisser, S. Landa, Sulfide Catalysts: Their Properties and Applications, Pergamon, Oxford, UK, 1973.
[2] H. Topsoe, B.S. Clausen, F.E. Massoth, Hydrotreating Catalysis Science and Technology, vol. 11, Springer Verlag, Berlin, 1996.
[3] J.A. Rodriguez, J. Dvorak, A.T. Capitano, A.M. Gabelnick, J.L. Gland, Surf. Sci. 429 (1999) L462–L468.
[4] G. Berhault, M. Lacroix, M. Breysse, F. Maugé, J.-C. Lavalley, H. Nie, L. Qu, J. Catal. 178 (1998) 555–565.
[5] M. Breysse, G. Berhault, S. Kasztelan, M. Lacroix, F. Maugé, G. Perot, Catal. Today 66 (2001) 13–20.
[6] R. Pis Diez, A.H. Jubert, J. Mol. Catal. 83 (1993) 219–325.
[7] (a) J.K. Nørskov, B.S. Clausen, H. Topsøe, Catal. Lett. 13 (1992) 1–8;
(b) H. Topsøe, B.S. Clausen, N.-Y. Topsøe, J.K. Nørskov, C.V. Ovesen, C.J.H. Jacobsen, Bull. Soc. Chim. Belg. 104 (1995) 283.
[8] (a) H. Toulhoat, G. Kresse, Am. Chem. Soc. Div. Petrol. Chem. Prepr. 42 (1997) 114;
(b) H. Toulhoat, P. Raybaud, S. Kasztelan, G. Kresse, J. Hafner, Catal. Today 50 (1999) 629–636.
[9] (a) T.A. Pecoraro, R.R. Chianelli, J. Catal. 67 (1981) 430–445;
(b) R.R. Chianelli, G. Berhault, P. Raybaud, S. Kasztelan, J. Hafner, H. Toulhoat, Appl. Catal. A: General 227 (2002) 83–96.
[10] R.R. Chianelli, M. Daage, M.J. Ledoux, Adv. Catal. 40 (1994) 117–232.
[11] S. Harris, R.R. Chianelli, J. Catal. 86 (1984) 400–412;
H. Toulhoat, P. Raybaud, J. Catal. 216 (2003) 63–72.
[12] J.P.R. Vissers, C.K. Groot, E.M. Vanoers, V.H.J. de Beer, Bull. Soc. Chim. Belg. 93 (1984) 813–821.
[13] M.J. Ledoux, O. Michaux, G. Agostini, P. Panisso, J. Catal. 102 (1986) 275–288.
[14] J.K. Burdett, J.T. Chung, Surf. Sci. Lett. 236 (1990) L353–L357.
[15] T.S. Smith, K.H. Johnson, Catal. Lett. 28 (1994) 361.
[16] P. Raybaud, G. Kresse, J. Hafner, H. Toulhoat, J. Phys.: Condens. Matter 9 (1997) 11085–11106.
[17] P. Raybaud, J. Hafner, G. Kresse, S. Kasztelan, H. Toulhoat, J. Catal. 190 (2000) 128–143.
[18] M. Neurock, R.A. van Santen, J. Am. Chem. Soc. 116 (1994) 4427–4439.
[19] Y. Aray, J. Rodriguez, D. Vega, E.N. Rodriguez-Arias, Angew. Chem. Int. Ed. 39 (2000) 3810–3813.
[20] B.S. Clausen, B. Lengeler, R. Candia, J. Als-Nielsen, H. Topsoe, Bull. Soc. Chim. Belg. 90 (1981) 1249–1259.
[21] T.G. Parham, R.P. Merrill, J. Catal. 85 (1984) 295–310.
[22] S.J. Tauster, T.A. Pecoraro, R.R. Chianelli, J. Catal. 63 (1980) 515–519.
[23] H. Topsoe, R. Candia, N.Y. Topsoe, B.S. Clausen, Bull. Soc. Chim. Belg. 93 (1984) 783–806.
[24] (a) J.V. Lauritsen, M.V. Bollinger, E. Lægsgaard, K.W. Jacobsen, J.K. Nørskov, B.S. Clausen, H. Topsøe, F. Besenbacher, J. Catal. 221 (2004) 510–522;
(b) H. Schweiger, P. Raybaud, H. Toulhoat, J. Catal. 212 (2002) 33–38;
(c) P. Raybaud, J. Hafner, G. Kresse, S. Kasztelan, H. Toulhoat, J. Catal. 189 (2000) 129–146;
(d) H. Schweiger, P. Raybaud, G. Kresse, H. Toulhoat, J. Catal. 207 (2002) 76–87.
[25] R.F.W. Bader, Atoms in Molecules–A Quantum Theory, Clarendon Press, Oxford, UK, 1990;
R.F.W. Bader, Chem. Rev. 91 (1991) 893.
[26] R.F.W. Bader, J. Phys. Chem. A 102 (1998) 7314–7323.
[27] R.F.W. Bader, P.L.A. Popelier, T.A. Keith, Angew. Chem., Int. Ed., Eng. 33 (1994) 620–631.
[28] P.F. Zou, R.F.W. Bader, Acta Crystallogr. A 50 (1994) 714–725.
[29] M.E. Eberhart, J. Can. Chem. Soc. 74 (1996) 1229–1235.
[30] M.E. Eberhart, Philos. Mag. A 73 (1996) 47–60.
[31] Y. Aray, J. Rodriguez, D. Vega, J. Phys. Chem. B 104 (2000) 4608–4612.
[32] M.A. Pendás, A. Costales, V. Luaña, Phys. Rev. B 55 (1997) 4275–4284.
[33] P. Popelier, Atoms in Molecules—An Introduction, Prentice Hall, Harlow-England, 2000.
[34] R.J. Gillespie, P.L.A. Popelier, Chemical Bonding and Molecular Geometry: From Lewis to Electrón Densities, Oxford University Press, New York, Oxford, 2001.
[35] N.E. Ghermani, C. Lecomte, Y. Dusausoy, Phys. Rev. B 53 (1996) 4231.
[36] C.L. Hénaff, N.K. Hansen, J. Protas, G. Marnier, Acta Crystallogr. B 53 (1997) 870.
[37] Y.V. Ivanov, E.L. Belokoneva, J. Protas, N.K. Hansen, V.G. Tirelson, Acta Crystallogr. B 54 (1998) 774.
[38] T.S. Koritsanszky, P. Coppens, Chem. Rev. 101 (2001) 1583.
[39] R.T. Downs, G.V. Gibbs, M.B. Boisen Jr., K.M. Rosso, Phys. Chem. Miner. 29 (2002) 369.
[40] Y.A. Abramov, F.P. Okamura, Acta Crystallogr. A 53 (1997) 187.
[41] M. Takata, M. Sakata, S. Kumazawa, F.K. Larsen, B. Iversen, Acta Crystallogr. A 50 (1994) 330.
[42] S.F. Vyboishchikov, A.E. Masunov, V.A. Streltsov, P.M. Zorkii, V.G. Tirelson, Zh. Fiz. Khim. 68 (1994) 2024.
[43] R. Boese, A.D. Boese, D. Blazer, M.Y. Antipin, A. Ellern, K. Seppelt, Angew. Chem. Int. Ed. Engl. 36 (1997) 1489.
[44] R. Boese, N. Niederprum, D. Blazer, A. Maulitz, M.Y. Antipin, P.R. Mallison, J. Phys. Chem. B 101 (1997) 5794.
[45] P. Munshi, T.N. Guru Row, Crystallogr. Rev. 11 (2006) 199.
[46] C.J. Mei, K.E. Edgecombe, V.H. Smith, A. Heilingbrunner, Int. J. Quant. Chem. 48 (1993) 287.
[47] Y. Aray, J. Rodríguez, J. Rivero, J. Phys. Chem. A 101 (1997) 6976.
[48] P. Mori-Sánchez, Densidad electrónica y enlace químico. De la molécula al cristal. Ph.D. Thesis, Universidad de Oviedo, 2002.
[49] M.E. Eberhart, D.P. Clougherty, J.M. MacLaren, J. Am. Chem. Soc. 115 (1993) 5762.
[50] M.E. Eberhart, D.P. Clougherty, J.M. MacLaren, J. Mater. Res. 8 (1993) 438.
[51] U. Haussermann, S. Wengert, R. Nesper, Angew. Chem. Int. Ed. Engl. 33 (1994) 2073.
[52] G.H. Grosch, K.J. Range, J. Alloys Compd. 233 (1996) 39.
[53] M. Knecht, H. Ebert, W. Bensch, J. Alloys Compd. 246 (1997) 166.
[54] V.G. Tirelson, P.F. Zou, T.H. Tang, R.F.W. Bader, Acta Crystallogr. A 51 (1995) 143.
[55] C. Gatti, V.R. Saunders, C. Roetti, J. Chem. Phys. 101 (1994) 10686.
[56] J.A. Plats, S.T. Howard, J. Chem. Phys. 105 (1996) 4668.
[57] V. Luaña, A. Costales, P. Mori-Sánchez, M.A. Pendás, J. Phys. Chem. B 107 (2003) 4912.
[58] M.A. Blanco, A. Costales, A.M. Pendás, V. Luaña, Phys. Rev. B 62 (2000) 12028.
[59] M.A. Pendás, A. Costales, V. Luaña, Phys. Rev. B 55 (1997) 4285.

[60] DMol^3 is Available as Part of Material Studio, Accelrys Inc., San Diego, USA, 2002.
[61] B. Delley, J. Chem. Phys. 92 (1990) 508;
B. Delley, J. Chem. Phys. 113 (2000) 7756.
[62] J.P. Perdew, K. Burke, M. Emzerhof, Phys. Rev. Lett. 77 (1996) 3865.
[63] Y. Aray, J.D. Rodriguez, Vega in The Quatum Theory of Atoms in Molecules: From DNA to Solid and Drug Design, C.F. Matta, R.J. Boyd (Eds), Wiley-VCH, Weinheim, 2006.
[64] K.D. Bronsema, J.L. De Boer, F. Jellinek, Z. Anorg. Allg. Chem. 540 (1986) 15–17.
[65] P. Raybaud, G. Kresse, H. Toulhoat, J. Phys. Condens. Matter. 9 (1997) 11085–11106.
[66] L.S. Byskov, J.K. Norskov, B.S. Clausen, H. Topsoe, Catal. Lett. 64 (2000) 95–99.
[67] L.S. Byskov, J.K. Norskov, B.S. Clausen, H. Topsoe, Catal. Lett. 47 (1997) 177–182.
[68] L.S. Byskov, J.K. Norskov, B.S. Clausen, H. Topsoe, J. Catal. 187 (1999) 109–122.
[69] S.M. Sun, J. Adjaye, A.E. Nelson, Appl. Catal. A: Gen. 263 (2004) 131–143.
[70] P. Raybaud, J. Hafner, H. Kresse, H. Toulhoat, Phys. Rev. Lett. 80 (1998) 1481–1484.
[71] P. Raybaud, J. Hafner, H. Kresse, H. Toulhoat, Surf. Sci. 407 (1998) 237–250.
[72] S. Cristol, J.F. Paul, E. Payen, D. Bougeard, F. Clemendot, F. Hutschka, J. Phys. Chem. 104 (2000) 11220–11229.
[73] J.F. Paul, E. Payen, J. Phys. Chem. B 107 (2003) 4057–4064.
[74] S. Cristol, J.F. Paul, E. Payen, D. Bougeard, F. Hutschka, J. Hafner, in: B. Delmond, J.F. Froment, P. Grange (Eds.), Proceedings of the Second International Symposium on Hydrotreatment and Hydrocracking of Oil Fractions, Stud. Surf. Sci. Catal. 127 (1999) 327.
[75] Y. Aray, J. Rodriguez, S. Coll, E. Rodríguez-Arias, D. Vega, J. Phys. Chem. B 109 (2005) 23564–23570.
[76] M. Leboeuf, M. Koster, K. Jug, D.R. Salahub, J. Chem. Phys. 111 (1999) 4893.
[77] S.R. Gadre, R.N. Shirsat, Electrostatics of Atoms and Molecules, Universities Press, Hyderabad, 2000.
[78] P. Politzer, D.G. Truhlar, Chemical Applications of Atomic and Molecular Electrostatic Potentials, Plenum, New York, 1982.
[79] J.S. Murray, K.D. Sen, Molecular Electrostatic Potential: Concepts and Applications, Elsevier, Amsterdam, 1996.
[80] M. Orozco, F.J. Luque, in: J.S. Murray, K.D. Sen (Eds.), Theoretical and Computational Chemistry Series, vol. 3, Elsevier, Amsterdam, 1996, p. 181.